HHS Public Access

Author manuscript

Biofabrication. Author manuscript; available in PMC 2015 December 01.

Published in final edited form as:

Biofabrication. ; 6(4): 045007. doi:10.1088/1758-5082/6/4/045007.

Additively Manufactured 3D Porous Ti-6Al-4V Constructs Mimic Trabecular Bone Structure and Regulate Osteoblast Proliferation, Differentiation and Local Factor Production in a Porosity and Surface Roughness Dependent Manner

Alice Cheng[1,2], **Aiza Humayun**[3], **David J. Cohen**[3], **Barbara D. Boyan**[1,3], and **Zvi Schwartz**[3,4]

[1]Wallace A. Coulter Department of Biomedical Engineering, Georgia Institute of Technology and Emory University, Atlanta, Georgia, USA

[2]Department of Biomedical Engineering, Peking University, Beijing, China

[3]Department of Biomedical Engineering, Virginia Commonwealth University, Richmond, Virginia, USA

[4]University of Texas Health Science Center at San Antonio, San Antonio, Texas, USA

Abstract

Additive manufacturing by laser sintering is able to produce high resolution metal constructs for orthopaedic and dental implants. In this study, we used a human trabecular bone template to design and manufacture Ti-6Al-4V constructs with varying porosity via laser sintering. Characterization of constructs revealed interconnected porosities ranging from 15–70% with compressive moduli of 2063–2954 MPa. These constructs with macro porosity were further surface-treated to create a desirable multi-scale micro-/nano-roughness, which has been shown to enhance the osseointegration process. Osteoblasts (MG63 cells) exhibited high viability when grown on the constructs. Proliferation (DNA) and alkaline phosphatase specific activity (ALP), an early differentiation marker, decreased as porosity increased, while osteocalcin (OCN), a late differentiation marker, as well as osteoprotegerin (OPG), vascular endothelial growth factor (VEGF) and bone morphogenetic proteins 2 and 4 (BMP2, BMP4) increased with increasing porosity. 3D constructs with the highest porosity and surface modification supported the greatest osteoblast differentiation and local factor production. These results indicate that additively manufactured 3D porous constructs mimicking human trabecular bone and produced with additional surface treatment can be customized for increased osteoblast response. Increased factors for osteoblast maturation and differentiation on high porosity constructs suggest the enhanced performance of these surfaces for increasing osseointegration *in vivo*.

Keywords

osteoblast differentiation; laser sintering; surface roughness; material properties; custom implants; additive manufacturing

*Corresponding Author: Barbara D. Boyan, Ph.D., School of Engineering, Virginia Commonwealth University, 601 West Main Street, Suite 331A, Richmond, Virginia 23284, Phone: 804-828-0190, bboyan@vcu.edu.

1. Introduction

Over two million dental implants are placed annually, and over four million hip and knee replacement surgeries are expected by the year 2030 [1, 2]. The orthopaedic implant market is projected to exceed $46 billion by the year 2017, in part due to an increasing number of elderly patients as well as increased quality of life expectations of younger patients [3]. Titanium and its alloys are still widely used in dental and orthopaedic metal implants, based on the ability of bone to form in tight apposition to implants fabricated from these materials [4–6]. Titanium and titanium-aluminum-vanadium (Ti6Al4V) have a naturally occurring passive oxide layer on their surface that is biologically preferable and resists corrosion, while still maintaining strong mechanical properties and a high strength to weight ratio [7].

Implant surface roughness is one factor that has been shown to successfully increase cell response *in vitro* and osseointegration *in vivo*, and micro-rough surfaces are currently used as the industry standard in dental and many bone-interfacing orthopaedic implants [8, 9]. Previous studies in our lab confirm that the combined presence of micro-/submicron-scale roughness contributes to increased osteoblast response [10, 11]. By altering only the surface microtopography and without exogenous factors in media, osteoblast differentiation can be increased on titanium surfaces [12]. This may be due in part to the protein-material interaction at the surface, which affects downstream cell response. Changes in the cytoskeleton, including integrin expression and signaling, have also been implicated in this effect [13, 14].

Although dental implant success is achieved in over 95% of healthy patients, certain risk factors still inhibit osseointegration. Osseointegration rates for diabetics and smokers are reduced tremendously [15, 16]. In addition, low bone density or osteoporosis most commonly seen in the increasing elderly population can also decrease osseointegration. Most orthopaedic implants have a lifetime of only 12–15 years, requiring revision surgery that can be fatal for older patients [5, 17]. These factors contribute to the need for improving both osseointegration rates and implant longevity. Therefore, there is an existing need for implants that have the ability to increase bone formation and enhance the regeneration process.

Titanium also has desirable mechanical properties due to its low modulus of elasticity and high strength to weight ratio [18]. However, solid titanium still exceeds the stiffness of cortical bone by more than threefold, causing stress shielding and bone loss downstream of the implant [19]. 3D porous coatings and implants have been proposed to decrease stress shielding via porosity-dependent mechanical properties and increased bone interlocking, making these a promising treatment for at risk patients or younger patients who need an extended implant lifetime [20, 21].

Additive manufacturing techniques provide a layer-by-layer approach to building porous or patient-specific implants that have tailored macro structural and mechanical properties [22]. Selective laser sintering (SLS) has the ability to create high resolution, porous metal constructs with positive results in both *in vitro* and *in vivo* studies [23]. There have been many studies that observe the effect of controlled porosity on *in vitro* or *in vivo* response.

However, porosity in these studies was created using homogeneous strut and pore sizing, without a biological template and limited surface modification [23–26]. Trabecular bone in the human body does not have the same pore shape, size or surface roughness. In studies where surface modification was used to induce micro-roughness, bulk porosity was limited to a user designed template [27, 28]. Thus far, the combination of macro structural parameters integrated with micro-scale surface treatment has not been studied. The purpose of this study was to replace the traditional man-made structural template with a biological template.

In this study, we used human trabecular bone as a template to laser sinter Ti6Al4V with varying porosity, and additionally modified the surfaces to obtain a combined micro-/nano-roughness. The resulting constructs were characterized for their surface, structural and mechanical properties. Cellular response to constructs with varying porosity was also performed, with the hypothesis that osteoblast response would increase on 3D constructs with increasing porosity.

2. Materials and Methods

2.1 Manufacturing

2.1.1 Material Manufacturing—A computed tomographic (CT) scan was taken of a human femoral head retrieved from a hip replacement (μCT 40, Scanco Medical, Bassersdorf, Switzerland) with a 16 μm voxel size. A template was created using Scanco software (Scanco Medical, Bassersdorf, Switzerland) and rotated and superimposed on itself 12, 24, or 36 times to create constructs with low (3DLP), medium (3DMP) and high porosity (3DHP), respectively (Figure 1A). Generated 3D renderings were manufactured into Ti6Al4V disks 15mm in diameter and 5mm in height. Each disk included a 1mm solid base upon which the remaining porous material was sintered in order to ensure mechanical stability during sintering. 2D surfaces were 15mm in diameter and 1mm in height (Figure 1B). Laser sintering was performed using an Ytterbium fiber laser system (EOS, EmbH Munchen, Germany) with Ti6Al4V (grade 5) particles 25–45um in diameter (Advanced Powders & Coatings, Quebec, Canada). Laser scanning speed was 7m/s with a wavelength of 1054nm, continuous power of 200W and laser spot size of 0.1mm.

2.1.2 Surface Modification—After manufacturing, disks were blasted with calcium phosphate particles using proprietary technology (AB Dental, Jerusalem, Israel) and then acid etched by ultrasonicating in 0.3N nitric acid (HNO_3) once for five minutes at 45°C and twice for five minutes at 25°C. Disks were rinsed in 97% methanol for five minutes. Final pickling treatment was performed by ultrasonicating disks thrice for 10 minutes in ultrapure distilled water, immersing for 30 minutes in 1:1 20 g/L NaOH to 20 g/L H2O2 for 30 minutes at 80°C and ultrasonicating in water for 10 minutes. Constructs were then placed in a degreaser for 12 minutes, immersed in 65% aqueous HNO3, and ultrasonicated thrice in water for 10 minutes. Surfaces were blotted with lint free tissue and allowed to dry for at least 24 hours in order to stabilize the oxide layer before characterization and cell culture.

2.2 Material Characterization

2.2.1 Surface Chemistry—Surface chemistry was analyzed using x-ray photoelectron spectroscopy (XPS, K-Alpha, ThermoFisher Scientific, Boston, MA). Samples were transferred to the analysis chamber at a pressure of 1e-8 mbar. An XR5 gun was used with a 500μm spot size at 15kV to perform survey scans with 20ms dwelling time and 1eV energy step size. Bulk chemistry was analyzed using energy dispersive x-ray spectroscopy (EDX, Hitachi SU-70, Tokyo, Japan).

2.2.2 Contact Angle—Sessile drop contact angle was used to assess surface energy and surface wettability (Ramé-Hart goniometer, Succasunna, NJ). 2D solid laser sintered surfaces that received the same post-processing treatment as 3D constructs (Figure 2E, F) were used as a proxy for contact angle measurements due to difficulty in obtaining accurate contact angle measurements for porous constructs. 4μl drops of distilled water were deposited on five predetermined locations per disk, with two disks per group (n=10). Videos of these drops were taken and still images were used in conjunction with DROPimage software (Ramé-Hart goniometer, Succasunna, NJ) to determine the average left and right contact angle of each drop.

2.2.3 Surface Topography—Surface topography was qualitatively assessed using scanning electron microscopy (SEM, Hitachi SU-70, Tokyo, Japan). Disks were secured on imaging stubs with carbon tape and imaged with 56μA ion current, 4kV accelerating voltage and 4mm working distance. Three locations per disk were imaged to ensure homogeneous assessment, with at least two disks per group imaged.

2.2.4 Roughness—Macro- and micro-roughness were analyzed with confocal laser microscopy (LEXT OLS4000, Olympus, Center Valley, PA). Macro roughness was analyzed with a 10x objective, and micro-roughness was analyzed with a 20x objective and additional 5x optical zoom. After a 3 point correction, a cutoff wavelength of 100μm was used to analyze average roughness (R_a) and surface area.

2.2.5 Porosity—3D constructs were analyzed for porosity using micro-computed tomography (micro CT) (SkyScan 1173, Micro Photonics, Inc., Allentown, PA). A volume of interest of 469mm^3, or approximately 66% of each construct's porous volume, was analyzed for total percent porosity, open porosity, pore diameter, strut size, and surface area to volume (SA/V) ratio. Scans were taken using an Al 1.0mm filter, 100kV voltage, 80μA current, 1120×1120 camera pixels, 0.2° rotation step, frame averaging of 10, random movement of 10. Post-processing included a global threshold of 100–255 and despeckling black and white speckles less than 10 voxels. We verified the validity of micro CT analysis by comparison of total porosity analyzed through a traditional method based on size and mass (Figure 1C).

2.2.5 Mechanical Testing—Compressive moduli of 3D constructs were determined using the MTS Insight 30 testing machine (MTS Systems, Minnesota, USA). A pre-load of 0.01kN was applied at 0.025 mm/s, then a test speed of 0.02 mm/s was used until failure or the maximum load of 30kN was applied. Data acquisition rate was 500Hz, and the

compressive modulus was taken as the slope output of the resulting stress/strain curve. Testing was performed on 6 constructs group (total n=6).

2.3 Biological Response

2.3.1 Cell Viability—The MG63 human osteoblast-like cell line was used as a model for osteoblast viability, proliferation and differentiation on sintered surfaces. These cells have been characterized and are used by our lab as a model for osteoblast response to titanium surfaces with varying topography [29, 30]. Surfaces were sterilized in UV for 20 minutes in a biosafety cabinet prior to cell culture. Cells were cultured in tissue culture polystyrene (TCPS) flasks until confluence, then centrifuged and resuspended to yield a plating density of 30,000 cells per cm^2 on TCPS, or 60,000 cells per surface in a 24-well plate. Dulbecco's modified Eagle medium (DMEM) with 10% fetal bovine serum (FBS) and 1% penicillin/streptomycin was used to feed cells 24 hours after plating and treat at confluence according to the TCPS control. 24 hours after confluence, cells were treated with 5 μM calcein-AM and 4 μM ethidium homodimer-1 (LIVE/DEAD, Life Technologies, California, USA) in 1x Dulbecco's phosphate buffered saline (D-PBS, Life Technologies) for 20 minutes. Surfaces were imaged using the Zeiss LSM 710 confocal microscope (Zeiss, Oberkochen, Germany). Individual images were taken of 2D disks, while 550um z-stacks were taken of 3D disks. Green (live) and red (dead) channel thresholds were optimized for each group in order to better distinguish cells. Three images were analyzed and averaged per z-stack, with at least n=6 total areas (z-stacks) analyzed for at least two constructs per group (total n=12).

2.3.2 Osteoblast Proliferation and Maturation—Surfaces were gamma irradiated prior to cell culture. MG63 cells were cultured as described above. Media were changed at confluence, and cells were harvested 24 hours after confluence, rinsed twice with 1xPBS, then stored at −20°C overnight for biological assays. Cell lysate was assayed for DNA content (P7589, Invitrogen) and total protein content (23225, Pierce). Alkaline phosphatase specific activity was measured as a function of *p*-nitrophenol production from *p*-nitrophenylphosphate at pH 10.2 and normalized to total protein. Media were assayed for osteocalcin (OCN, BT-480, Biomedical Technologies, Inc.), VEGF (DY293B, R&D Systems), OPG (DY805, R&D Systems), BMP2 (900-K255, PeproTech) and BMP4 (DY 314, R&D Systems). Data were normalized to total DNA content. Experiments were performed at least twice to ensure validity of the results.

2.3.3 Sample Preparation for Scanning Electron Microscopy—One disk from each group was UV-treated for 20 minutes in a biological hood and plated with 60,000 MG63 cells and cultured as described above. Media were changed at confluence, and cells were fixed 24 hours after confluence with 4% paraformaldehyde (Electron Microscopy Sciences). Constructs were rinsed three times in 1xPBS, then dehydrated in a series of increasing ethanol concentrations: 15%, 30%, and 45% for two hours, then 60%, 75%, 90% and thrice in 100% for at least one hour. Samples were then exchanged in 1:1 100% ethanol and hexamethyldisilazane (HMDS, Sigma Aldrich) for 30 minutes in a chemical safety hood, then twice in 100% HMDS for 30 minutes. Samples were dried 24 hours in a desiccator before being platinum sputtered and imaged with SEM as described above (Hitachi SU-70, Tokyo, Japan).

2.4 Statistical Analysis

Surface characterization data are presented as mean ± one standard deviation (SD) of all measurements performed across samples in the same group. Cell viability is presented as the mean of all measurements performed across samples in the same group. Cell proliferation and differentiation data are presented as mean ± standard error of the mean (SEM) for six independent cultures. All experiments were repeated at least twice to ensure validity of observations, with results from individual experiments shown. Statistical analysis among groups was performed by analysis of variance, and significant differences between groups were compared using Bonferroni's modification of Student's t-test. A p value of less than 0.05 was considered statistically significant.

3. Results

3.1 Surface Characterization

Laser sintered 3DLP, 3DMP and 3DHP constructs had 16.2±2.9%, 38.5±3.9%, and 70.0±3.5% total porosity and 15.0±2.9%, 37.9±4.0%, 70.0±3.5% open porosity, respectively (Table 1). Total porosity and open porosity were not significantly different, showing complete interconnectivity between pores (Figure 1D). Average pore diameter was 177±22 μm for 3DLP, 383±15 μm for 3DMP and 653±22 μm for 3DHP constructs. Average strut thickness was 628±150 μm for 3DLP, 454±57 μm for 3DMP and 305±26 μm for 3DHP. The ratio between the analyzed construct surface area to volume ratio was 23.5 ± 7.4 for 3DLP, 36.1 ± 5.4 for 3DMP, and 56.9 ± 5.8 for 3DHP disks. For all porosity parameters (total porosity, open porosity, pore diameter, strut thickness and SA/V ratio), all groups were significantly different from each other. Pore diameter, strut thickness and SA/V ratio all increased with increasing construct porosity.

Surface chemistry performed by XPS showed mostly C, O and Ti in the oxide layer, with small amounts of N, P and Ca due to processing, and Al present on 2D surfaces (Table 2). EDX allows for higher penetration past the oxide layer and showed Ti, Al and V as the bulk surface composition, with a small amount of C present on 3DLP surfaces (Table 3). Contact angle of 2D proxy surfaces was 92 degrees with a standard deviation of 8 degrees. Compressive modulus decreased in a porosity-dependent manner (Table 4). 3DLP had a modulus of 2954±21, 3DMP a modulus of 2818±42 MPa and 3DHP a modulus of 2063±85.

After manufacturing the surfaces had a very grainy topography at the macro scale, but smooth topography at the micro scale (Figure 2A, B). Blasting and acid etching induced micro roughness on surfaces while maintaining macro structure (Figure 2C, D). Pickling overlaid fine and homogenous nanofeatures on the macro surface (Figure 2E, F). Cross sectional, low magnification SEM images show internal pore surfaces looking similar to pretreated constructs, indicating the inability of grit blasting treatment to affect internal construct pores (Figure 3). Surface roughness results revealed increasing surface roughness and area at the macro level for increasing porosity (Figure 4A, B). Surface micro roughness showed no difference between groups except an elevation in 3DHP surfaces, and no difference between groups for surface area at the micro level (Figure 4C, D).

3.2 Biological Response

Live/dead analysis indicated that cells on all surfaces had high viability. No significant differences in osteoblast viability were observed across constructs with varying porosity (Figure 5A). 2D surfaces had the highest percent viability at 99.9%. 3DLP, 3DMP and 3DHP constructs had 94.9%, 98.1% and 91.6% cell viability, respectively. A noticeable decrease in number of cells was seen on 2D surfaces cultured under continuously shaking conditions. Representative SEM micrographs of cells cultured on disks showed cells spread evenly across surfaces (Figure 5B).

DNA was highest on TCPS and decreased as porosity increased (Figure 6A). ALP, a marker of early osteoblastic differentiation, was elevated on 3DLP compared to TCPS, then decreased on 3DMP and 3DHP compared to 3DLP, and decreased significantly on 3DHP compared to TCPS (Figure 6B). OCN increased significantly on 3DHP compared to TCPS (Figure 6C). OPG increased on 3DMP and 3DHP compared to TCPS and 3DLP, and was also significantly higher on 3DHP compared to 3DMP (Figure 6D). BMP2 on 3DLP, 3DMP and 3DHP was significantly higher than on TCPS, and 3DMP and 3DHP constructs had higher BMP2 levels compared to 3DLP (Figure 6E). BMP4 was elevated on 3DHP compared to TCPS only (Figure 6F). VEGF was elevated on 3DMP and 3DHP compared to TCPS and 3DLP, and was also significantly higher on 3DHP compared to 3DMP (Figure 6G).

4. Discussion

Increased implant failure due to lack of osseointegration is a problem in compromised patients, which creates the need for better bone integration and mechanical properties of Ti and Ti alloy implants [16]. Although studies have pointed toward 3D porous implants as a possible solution, these surfaces have not been optimized for porosity or combined with desired surface roughness features.

Various additive manufacturing methods such as direct beam melting and laser sintering have come to the forefront of customized and porous implant manufacturing. The sintering system we use in this study has a theoretical resolution of 100 microns according to the laser size; however, limited studies have been performed on the homogeneity of laser strength within that diameter. Scan speed and wavelength can all have an effect on the manufactured structure’s density and therefore mechanical properties, but with higher resolution comes increased time of production.

Previous studies have observed increased sintering density of over 97% with decreasing scan speeds to 50 mm/s [24]. Our qualitative evaluations using SEM and quantitative analysis using micro CT point toward a close approximation of our construct structure with that of human trabecular bone, even at high density. Although the optimal pore diameter for porous implants has been debated in literature, most studies observe increased cell infiltration or bone ingrowth for pores larger than 100μm in diameter [31–33]. Pore sizes of 200–400μm have been thought to increase osteoblast attachment, migration and proliferation via activation of mechanoreceptors [34]. We observed pore sizes upwards of 300μm in our disks, which has been suggested as a minimum for new bone and capillary formation [33].

Pore diameter has been suggested to have higher influence on bone ingrowth when compared to total percent porosity alone, although we were not able to isolate these two variables in our constructs [35].

Similar processing methods have previously been shown to successfully manufacture surfaces with stable mechanical properties and good *in vitro* results [27]. The effect of roughness at both the micro- and nano-scales on osteoblast differentiation has been well documented [10, 29, 36], and our results show that traditional methods such as blasting and acid etching are effective at inducing a homogeneous combined micro-/nano-roughness on additively manufactured surfaces. Due to the high interconnectivity between pores, acid treatment and pickling solutions were able to access the entire surface area of constructs to create a unique, homogenous nanostructured surface. However, our results show that blasting was not able to significantly alter the internal pores of the constructs. Despite this, cell response still increased significantly for high porosity constructs, suggesting that macro-structural effects of 3D porous constructs may play a larger role in cell response compared to surface roughness alone.

Human trabecular bone from the mandible has a porosity range of 70–90%, which varies with location and patient factors [37–39]. In this study, we created porous structures ranging from 20–70% to determine the optimal percent porosity for cells. Our compressive moduli decrease with increasing porosity, which has been corroborated for both synthetic constructs and human bone [20, 38]. Compressive testing on human trabecular bone has shown a compressive modulus of 1.08 GPa [40]. A study encompassing 160 human trabecular bone samples with compressive moduli ranging from approximately 300–900 MPa showed that bone-volume fraction (density), surface-to-volume ratio, trabecular thickness (strut thickness) and spacing (pore diameter) all contributed significantly to differences in mechanical properties [41]. The direction of loading can also impact mechanical output, which is especially true due to the anisotropic properties of bone [25]. In this study, we performed testing on porous constructs with a 1mm solid base, which may have contributed to a higher modulus than just the porous component alone.

Surface chemistry of disks with varying porosity contained mainly elements of Ti, O and C, although bulk chemistry confirmed the presence of Ti, Al and V in the alloy. Previous surface analysis of Ti6Al4V surfaces has also shown the presence of Al in the oxide layer, which may have been masked by Ca and P after blasting [42]. Contact angle on 2D proxy surfaces was neither super-hydrophilic nor hydrophobic. These 2D surfaces underwent the same surface treatment as 3D constructs, although the effect of strut curvature and differences in internal surface roughness on wettability for 3D constructs could not be determined. Surface roughness and area at the micro level were not different among groups except for an elevated roughness on 3DHP, which may have been due to the decreased strut thickness and increased curvature at sites of analysis.

Cell viability was high and not significantly different among surfaces. A qualitative observation of a decrease in cell number with increasing porous constructs suggests that cells had infiltrated pores and distributed over a larger surface area. Previous studies on additively manufactured porous surfaces also showed high cell viability and cell infiltration

into pores [43], which were confirmed by our SEM images. We assume high cell viability exists for cells that have infiltrated to the pores; however, we were not able to visualize all the way to the bottom of the disks to fully verify cell infiltration. Viability results were limited to the first 550μm, a limitation of the imaging equipment.

The decrease in ALP specific activity and the increase in OCN point toward a porosity-dependent maturation response. Previous reports of ALP activity on roughened surfaces noted a significant difference in cell layer activity versus isolated cells, suggesting increased matrix vesicle production [44]. These results also correspond to the decreased DNA content on 3DHP constructs, indicating a preference toward osteoblast maturation instead of proliferation. OPG, a decoy receptor for RANKL and involved in the bone remodeling process, was increased on 3DMP and 3DHP constructs. This increase in OPG blocks osteoclast differentiation in a protective effect to enhance bone growth, and has been implicated in osteoblast-osteoclast communication [45]. An increase of BMP2 and BMP4, especially on 3DHP surfaces, corroborates previous studies that observe increased BMP production on constructs with 300–400μm pore diameters [46]. Although our pore diameters are larger, the irregular porosity of trabecular bone may contribute differently to local factor production than in other studies with user-defined geometries. The increase of BMP local factor production indicates that our porous constructs have the potential to regulate the induction of bone inside the construct, as well as induce bone distally. The Increased levels of VEGF on 3DHP constructs also point toward this trend, indicating that highly porous constructs of trabecular bone structure are inductive for blood vessel formation as part of supporting new bone formation and bone regeneration.

As percent porosity increased, so did the surface area to volume ratio, indicating an increased surface area for cell interaction. It has previously been shown that rough titanium surfaces enhance osteoblastic differentiation and increase local factor production, so the increased cell response in this study may well be attributed to the varying material properties of our surface [30]. In this study, the combination of the three dimensional macro-structure, increase in surface area and combined micro-/nano- surface modification enhanced the osteoblast phenotype. Increased curvature on 3D surfaces with higher porosity may exert higher mechanical forces on a cell, which has been shown to direct cells toward osteoblast differentiation [47]. This response could be mediated by cell-surface integrin proteins. In particular, $\alpha 5$ has been implicated in osteoblast attachment and proliferation, and $\alpha 2\beta 1$ in osteoblast morphology and differentiation via its binding to collagen in the extracellular matrix [13, 48].

The role of confluence may contribute to cell response, and has been previously discussed with regard to TCPS versus rough titanium surfaces [49]. Although decreased DNA was shown on Ti6Al4V surfaces compared to TCPS controls, previous studies on pre-confluent cultures have also shown a different maturation profile of osteoblasts on the Ti alloy surfaces compared to TCPS, suggesting that our resulting cell response was also surface specific and not confluence dependent [34].

Increased bone growth in response to additively manufactured implants has been shown in various animal models, including rats and sheep [28, 50]. Previous work has shown highest

calcium content and *in vivo* response to materials with 75% porosity compared to higher porosities [51]. Further work in an animal model will be essential to assess the success of bone growth into individual pores and osseointegration capability of the entire porous construct.

5. Conclusion

In this study, we used additive manufacturing to produce Ti6AlV materials with varying porosity that structurally mimicked human trabecular bone, and further created a desirable surface for osteoblasts by inducing combined micro-/nano-roughness. Our results indicate that a high porosity construct mimicking trabecular bone structure is capable of stimulating osteoblast differentiation when compared to 2D and low porosity constructs. Additive manufacturing is a scalable manufacturing method that has the potential to create structurally complex, patient-specific orthopaedic and dental implants and scaffolds for increased osseointegration. Although trabecular orientation may vary across individuals and locations in the body, this study suggests that osteoblast cells actually do prefer one type of porosity and structure. In addition, this study reveals the possibility for creating patient-specific implants, which may accelerate the fields of dental and orthopaedic implants.

Acknowledgments

The authors would like to thank AB Dental (Jerusalem, Israel) for funding this study. The authors also recognize the support of the National Science Foundation (AC) and the National Institutes of Health (US PHS Grant AR052102, BDB).

References

1. Kurtz S, Ong K, Lau E, Mowat F, Halpern M. Projections of primary and revision hip and knee arthroplasty in the United States from 2005 to 2030. J Bone Joint Surg Am. 2007; 89:780–5. [PubMed: 17403800]
2. The 2005–06 Survey of Dental Services Rendered. Chicago, IL: American Dental Association; 2007.
3. Industry Experts. 2011. Orthopedic Implants - A Global Market Overview.
4. Van Noort R. Titanium: the implant material of today. Journal of Materials Science. 1987; 22:3801–11.
5. Rack H, Qazi J. Titanium alloys for biomedical applications. Materials Science and Engineering: C. 2006; 26:1269–77.
6. Long M, Rack HJ. Titanium alloys in total joint replacement—a materials science perspective. Biomaterials. 1998; 19:1621–39. [PubMed: 9839998]
7. Textor, M.; Sittig, C.; Frauchiger, V.; Tosatti, S.; Brunette, DM. Titanium in medicine. Springer; 2001. Properties and biological significance of natural oxide films on titanium and its alloys; p. 171-230.
8. Zhao G, Zinger O, Schwartz Z, Wieland M, Landolt D, Boyan BD. Osteoblast-like cells are sensitive to submicron-scale surface structure. Clinical Oral Implants Research. 2006; 17:258–64. [PubMed: 16672020]
9. Zinger O, Zhao G, Schwartz Z, Simpson J, Wieland M, Landolt D, et al. Differential regulation of osteoblasts by substrate microstructural features. Biomaterials. 2005; 26:1837–47. [PubMed: 15576158]
10. Gittens R, McLachlan T, Cai Y, Berner S, Tannenbaum R, Schwartz Z, et al. The effects of combined micron-/submicron-scale surface roughness and nanoscale features on cell proliferation and differentiation. Biomaterials. 2011; 32:3395–403. [PubMed: 21310480]

11. Zhao G, Raines AL, Wieland M, Schwartz Z, Boyan BD. Requirement for both micron- and submicron scale structure for synergistic responses of osteoblasts to substrate surface energy and topography. Biomaterials. 2007; 28:2821–9. [PubMed: 17368532]
12. Olivares-Navarrete R, Hyzy SL, Hutton DL, Erdman CP, Wieland M, Boyan BD, et al. Direct and indirect effects of microstructured titanium substrates on the induction of mesenchymal stem cell differentiation towards the osteoblast lineage. Biomaterials. 2010; 31:2728–35. [PubMed: 20053436]
13. Olivares-Navarrete R, Raz P, Zhao G, Chen J, Wieland M, Cochran DL, et al. Integrin α2β1 plays a critical role in osteoblast response to micron-scale surface structure and surface energy of titanium substrates. Proceedings of the National Academy of Sciences. 2008; 105:15767–72.
14. Keselowsky BG, Wang L, Schwartz Z, Garcia AJ, Boyan BD. Integrin α5 controls osteoblastic proliferation and differentiation responses to titanium substrates presenting different roughness characteristics in a roughness independent manner. Journal of Biomedical Materials Research Part A. 2007; 80A:700–10. [PubMed: 17133443]
15. Bain CA, Moy PK. The Association Between the Failure of Dental Implants and Cigarette Smoking. International Journal of Oral & Maxillofacial Implants. 1993; 8:1–13.
16. Moy PK, Medina D, Shetty V, Aghaloo TL. Dental Implant Failure Rates and Associated Risk Factors. International Journal of Oral & Maxillofacial Implants. 2005; 20:569–77. [PubMed: 16161741]
17. Mahomed NN, Barrett JA, Katz JN, Phillips CB, Losina E, Lew RA, et al. Rates and Outcomes of Primary and Revision Total Hip Replacement in the United States Medicare Population. The Journal of Bone & Joint Surgery. 2003; 85:27–32. [PubMed: 12533568]
18. Lautenschlager EP, Monaghan P. Titanium and titanium alloys as dental materials. International dental journal. 1993; 43:245–53. [PubMed: 8406955]
19. Sumner DR, Turner TM, Igloria R, Urban RM, Galante JO. Functional adaptation and ingrowth of bone vary as a function of hip implant stiffness. Journal of biomechanics. 1998; 31:909–17. [PubMed: 9840756]
20. Parthasarathy J, Starly B, Raman S, Christensen A. Mechanical evaluation of porous titanium (Ti6Al4V) structures with electron beam melting (EBM). Journal of the Mechanical Behavior of Biomedical Materials. 2010; 3:249–59. [PubMed: 20142109]
21. Sumner DR, Galante JO. Determinants of stress shielding: design versus materials versus interface. Clin Orthop Relat Res. 1992:202–12. [PubMed: 1729005]
22. van Noort R. The future of dental devices is digital. Dental Materials. 2012; 28:3–12. [PubMed: 22119539]
23. Warnke PH, Douglas T, Wollny P, Sherry E, Steiner M, Galonska S, et al. Rapid prototyping: porous titanium alloy scaffolds produced by selective laser melting for bone tissue engineering. Tissue engineering Part C, Methods. 2009; 15:115–24. [PubMed: 19072196]
24. Bertol LS, Júnior WK, Silva FPd, Aumund-Kopp C. Medical design: Direct metal laser sintering of Ti–6Al–4V. Materials & Design. 2010; 31:3982–8.
25. Heinl P, Müller L, Körner C, Singer RF, Müller FA. Cellular Ti–6Al–4V structures with interconnected macro porosity for bone implants fabricated by selective electron beam melting. Acta Biomaterialia. 2008; 4:1536–44. [PubMed: 18467197]
26. Ryan G, Pandit A, Apatsidis DP. Fabrication methods of porous metals for use in orthopaedic applications. Biomaterials. 2006; 27:2651–70. [PubMed: 16423390]
27. Traini T, Mangano C, Sammons R, Mangan F, Macchi A, Piettelli A. Direct laser metal sintering as a new approach to fabrication of an isoelastic functionally graded material for manufacture of porous titanium dental implants. Dental Materials. 2008; 24:1525–33. [PubMed: 18502498]
28. Amin Yavari S, van der Stok J, Chai YC, Wauthle R, Tahmasebi Birgani Z, Habibovic P, et al. Bone regeneration performance of surface-treated porous titanium. Biomaterials. 2014; 35:6172–81. [PubMed: 24811260]
29. Lincks J, Boyan BD, Blanchard CR, Lohmann CH, Liu Y, Cochran DL, et al. Response of MG63 osteoblast-like cells to titanium and titanium alloy is dependent on surface roughness and composition. Biomaterials. 1998; 19:2219–32. [PubMed: 9884063]

30. Schwartz Z, Raz P, Zhao G, Barak Y, Tauber M, Yao H, et al. Effect of Micrometer-Scale Roughness of the Surface of Ti6Al4V Pedicle Screws in Vitro and in Vivo. The Journal of Bone & Joint Surgery. 2008; 90:2485–98. [PubMed: 18978418]
31. Xue W, Krishna BV, Bandyopadhyay A, Bose S. Processing and biocompatibility evaluation of laser processed porous titanium. Acta Biomaterialia. 2007; 3:1007–18. [PubMed: 17627910]
32. Jones AC, Arns CH, Sheppard AP, Hutmacher DW, Milthorpe BK, Knackstedt MA. Assessment of bone ingrowth into porous biomaterials using MICRO-CT. Biomaterials. 2007; 28:2491–504. [PubMed: 17335896]
33. Karageorgiou V, Kaplan D. Porosity of 3D biomaterial scaffolds and osteogenesis. Biomaterials. 2005; 26:5474–91. [PubMed: 15860204]
34. Boyan BD, Hummert TW, Dean DD, Schwartz Z. Role of material surfaces in regulating bone and cartilage cell response. Biomaterials. 1996; 17:137–46. [PubMed: 8624390]
35. Gauthier O, Bouler J-M, Aguado E, Pilet P, Daculsi G. Macroporous biphasic calcium phosphate ceramics: influence of macropore diameter and macroporosity percentage on bone ingrowth. Biomaterials. 1998; 19:133–9. [PubMed: 9678860]
36. Martin JY, Schwartz Z, Hummert TW, Schraub DM, Simpson J, Lankford J Jr, et al. Effect of titanium surface roughness on proliferation, differentiation, and protein synthesis of human osteoblast-like cells (MG63). Journal of biomedical materials research. 1995; 29:389–401. [PubMed: 7542245]
37. Misch CE, Qu Z, Bidez MW. Mechanical properties of trabecular bone in the human mandible: implications for dental implant treatment planning and surgical placement. Journal of oral and maxillofacial surgery : official journal of the American Association of Oral and Maxillofacial Surgeons. 1999; 57:700–6. discussion 6–8.
38. McCalden RW, McGeough JA, Barker MB, Court-Brown CM. Age-related changes in the tensile properties of cortical bone. The relative importance of changes in porosity, mineralization, and microstructure. The Journal of Bone & Joint Surgery. 1993; 75:1193–205. [PubMed: 8354678]
39. Seeman E. Pathogenesis of bone fragility in women and men. The Lancet. 2002; 359:1841–50.
40. Sevilla P, Aparicio C, Planell JA, Gil FJ. Comparison of the mechanical properties between tantalum and nickel–titanium foams implant materials for bone ingrowth applications. Journal of Alloys and Compounds. 2007; 439:67–73.
41. Ding M, Odgaard A, Danielsen CC, Hvid I. Mutual associations among microstructural, physical and mechanical properties of human cancellous bone. The Journal of bone and joint surgery. 2002; 84:900–7. British volume. [PubMed: 12211688]
42. Gittens RA, Olivares-Navarrete R, McLachlan T, Cai Y, Hyzy SL, Schneider JM, et al. Differential responses of osteoblast lineage cells to nanotopographically-modified, microroughened–titanium–aluminum vanadium alloy surfaces. Biomaterials. 2012; 33:8986–94. [PubMed: 22989383]
43. Hollander DA, von Walter M, Wirtz T, Sellei R, Schmidt-Rohlfing B, Paar O, et al. Structural, mechanical and in vitro characterization of individually structured Ti–6Al–4V produced by direct laser forming. Biomaterials. 2006; 27:955–63. [PubMed: 16115681]
44. Kieswetter K, Schwartz Z, Dean DD, Boyan BD. The role of implant surface characteristics in the healing of bone. Critical reviews in oral biology and medicine : an official publication of the American Association of Oral Biologists. 1996; 7:329–45.
45. Boyce BF, Xing L. Biology of RANK, RANKL, and osteoprotegerin. Arthritis research & therapy. 2007; 9 (Suppl 1):S1. [PubMed: 17634140]
46. Tsuruga E, Takita H, Itoh H, Wakisaka Y, Kuboki Y. Pore Size of Porous Hydroxyapatite as the Cell-Substratum Controls BMP-Induced Osteogenesis. Journal of Biochemistry. 1997; 121:317–24. [PubMed: 9089406]
47. Kilian KA, Bugarija B, Lahn BT, Mrksich M. Geometric cues for directing the differentiation of mesenchymal stem cells. Proceedings of the National Academy of Sciences. 2010; 107:4872–7.
48. Lai M, Hermann CD, Cheng A, Olivares-Navarrete R, Gittens RA, Bird MM, et al. Role of α2β1 Integrins in Mediating Cell Shape on Microtextured Titanium Surfaces. Journal of Biomedical Materials Research Part A. 2014 n/a-n/a.

49. Kieswetter K, Schwartz Z, Hummert TW, Cochran DL, Simpson J, Dean DD, et al. Surface roughness modulates the local production of growth factors and cytokines by osteoblast-like MG-63 cells. Journal of biomedical materials research. 1996; 32:55–63. [PubMed: 8864873]

50. Stubinger S, Mosch I, Robotti P, Sidler M, Klein K, Ferguson SJ, et al. Histological and biomechanical analysis of porous additive manufactured implants made by direct metal laser sintering: A pilot study in sheep. Journal of Biomedical Materials Research Part B: Applied Biomaterials. 2013; 101:1154–63.

51. Bandyopadhyay A, Espana F, Balla VK, Bose S, Ohgami Y, Davies NM. Influence of porosity on mechanical properties and in vivo response of Ti6Al4V implants. Acta Biomaterialia. 2010; 6:1640–8. [PubMed: 19913643]

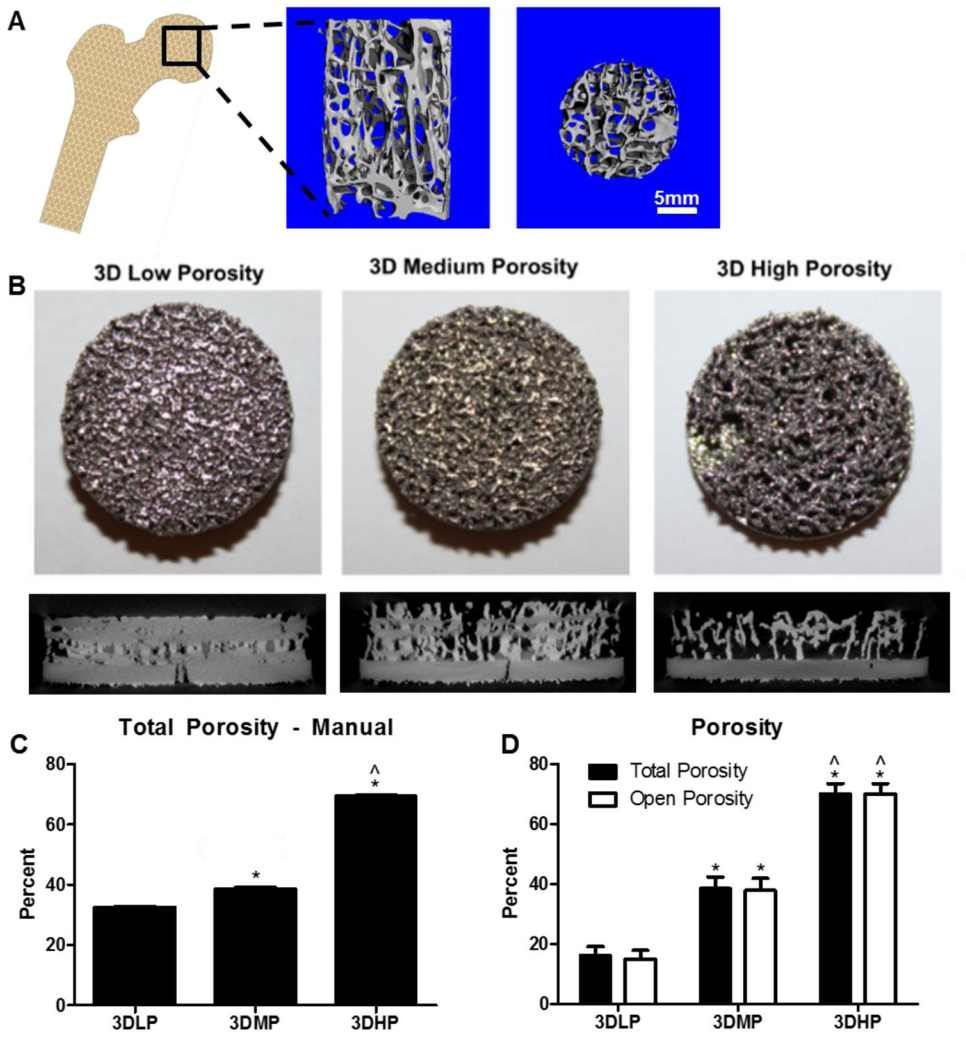

Figure 1.

(Left to right) Laser sintered disks were created from a CT scan conducted of human trabecular bone from the femoral head after a hip replacement. Original CT scans showing bone porosity through transverse and axial cross sections were used as a template for porous, laser sintered disks (A). Top-down camera images and micro CT cross sections of laser sintered 3D disks with (from left to right) low, medium and high porosity (B). Total porosity was calculated using a traditional method based on mass (C). Total and open porosity was calculated with micro CT (D). 1 way ANOVA with Bonferroni's correction was performed separately for total porosity or open porosity. $p<0.05$ is indicated by * vs. 3DLP and ^ vs. 3DMP. Unpaired t-test between total and open porosity showed no significance between groups.

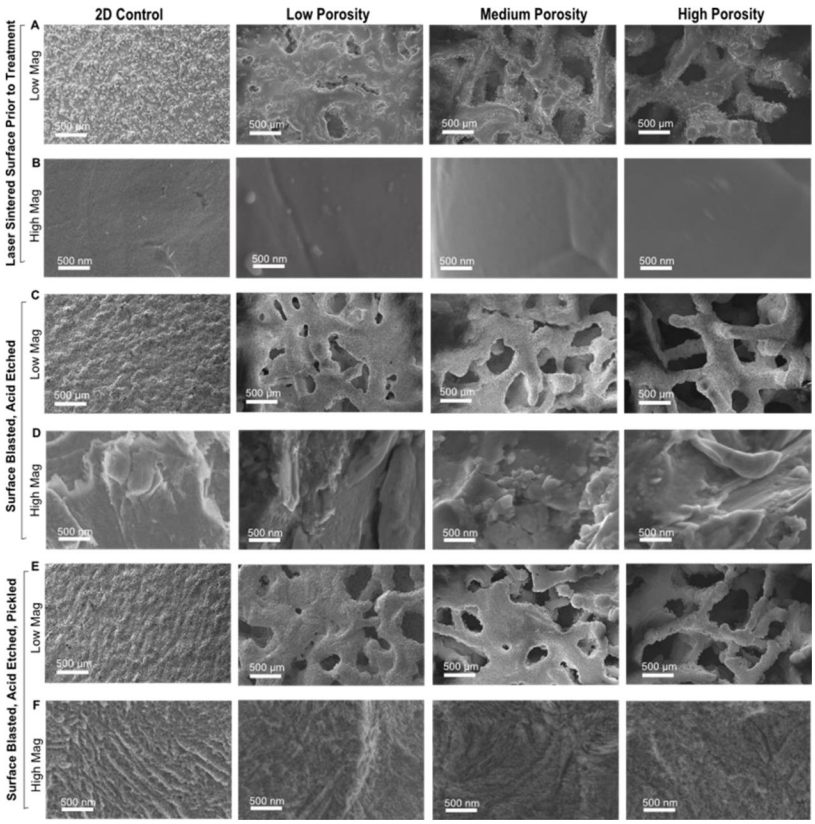

Figure 2.

SEM images of (columns from left to right) 2D, 3D low, medium and high porosity disks. Low magnification images showing trabecular structure after production (A), after blasting and acid etching (B), and after picking (C). High magnification images showing smooth surfaces after production (B), micro-roughness after blasting and acid etching (D), and nano-roughness after pickling (F).

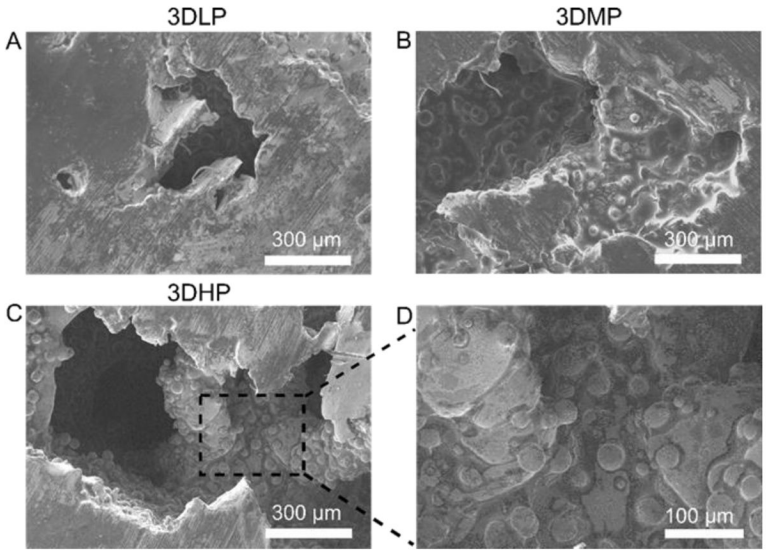

Figure 3.

Cross sectional SEM images of 3DLP (A); 3DMP (B); and 3DHP (C) constructs. An enlarged image of 3DHP (D) shows an absence of surface roughness induced by grit blasting.

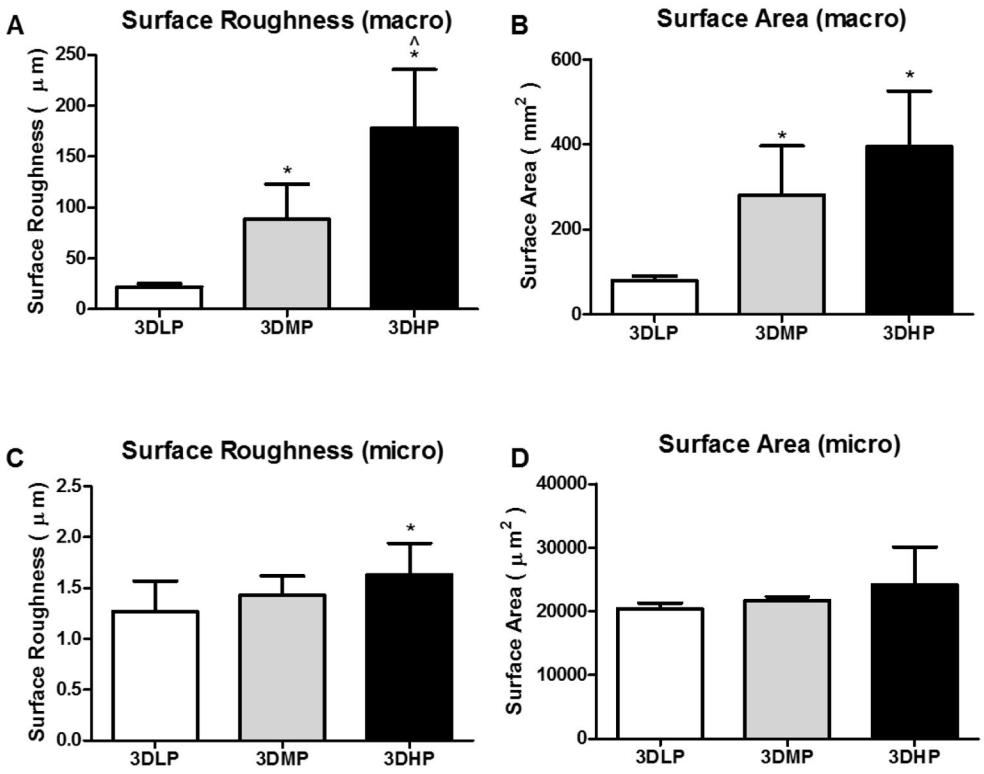

Figure 4.

Macro surface roughness (A), macro surface area (B), micro surface roughness (C) and micro surface area (D) analyzed with laser confocal microscopy. 1 way ANOVA with Bonferroni's correction shows significance of $p<0.05$ for * vs. 3DLP and ^ vs. 3DMP.

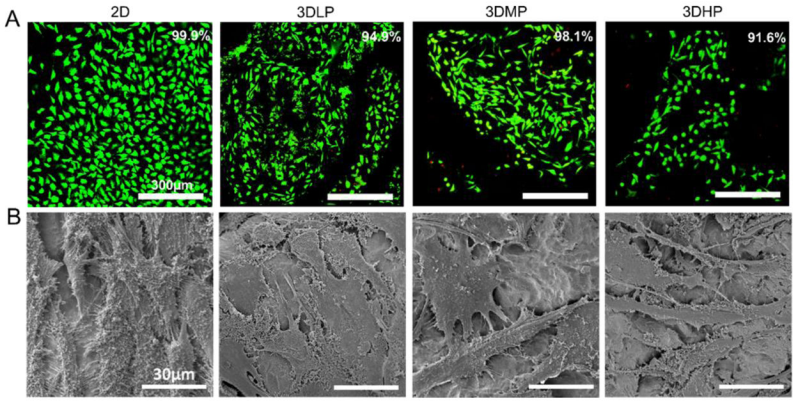

Figure 5.

MG63 cell viability (live=green, dead=red) after culturing until confluence on TCPS (A). No differences were found among groups using 1 way ANOVA with Bonferroni's correction, $p<0.05$. SEM micrographs revealing well-spread cell morphology on surfaces (B).

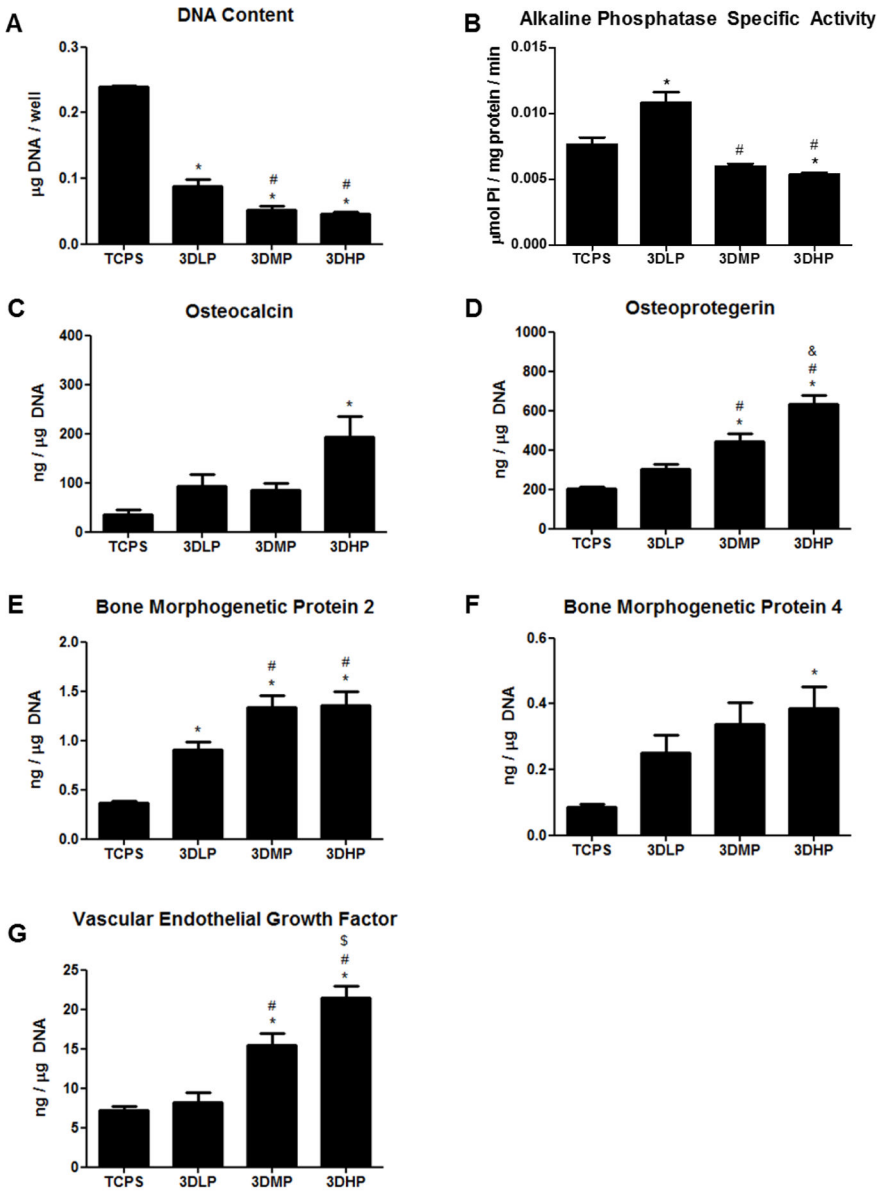

Figure 6.

MG63 cell response to laser sintered, porous surfaces 24 hours after confluence. DNA content (A), alkaline phosphatase specific activity (B), osteocalcin (C), osteoprotegerin (D), bone morphogenetic protein 2 (E), bone morphogenetic protein 4 (F), and vascular endothelial growth factor (G). Significance determined with 1 way ANOVA with Bonferroni's post- correction, $p<0.05$ for * vs. TCPS, ^ vs. 2D, # vs. 3DLP and $ vs. 3D-MP.

Table 1

Porosity Parameters

Porosity Parameters (Average ± SD)					
	Total Porosity (%)	**Open Porosity (%)**	**Pore Diameter (μm)**	**Strut Thickness (μm)**	**SA/V Ratio**
3DLP	16.2 ± 2.9	15.0 ± 2.9	177 ± 22	628 ± 150	23.5 ± 7.4
3DMP	38.5 ± 3.9 (*)	37.9 ± 4.0 (*)	383 ± 15 (*)	454 ± 57 (*)	36.1 ± 5.4 (*)
3DHP	70.0 ± 3.5 (*^)	70.0 ± 3.5 (*^)	653 ± 22 (*^)	305 ± 26 (*^)	56.9 ±5.8 (*^)

Significance

* vs. LP,

^ vs. MP $p<0.05$.

Table 2

Surface Chemistry (XPS): Elemental Composition

Element (Atomic % Average ± SD)							
	O	**C**	**Ti**	**N**	**P**	**Ca**	**Al**
2D	41.6 ± 3.7	41.8 ± 5.4	12.6 ± 1.5	1.3 ± 0.6	--	--	2.5 ± 0.5
3D-LP	44.9 ± 4.4	36.6 ± 7.9	6.3 ± 1.7	5.6 ± 1.5	3.3 ± 3.9	2.6 ± 1.9	--
3D-MP	54.5 ± 1.9	20.5 ± 20.4	6.9 ± 1.7	4.9 ±0.9	9.7 ± 1.6	3.6 ± 1.0	--
3D-HP	51.7 ± 3.1	29.5 ± 2.8	13.4 ± 1.1	3.2 ± 0.8	1.6 ± 1.8	--	--

Does not include trace elements less than 1%

Table 3

Surface Chemistry (EDX): Elemental Composition

Element (Weight % Average ± SD)				
	Ti	**Al**	**V**	**C**
2D	89.8 ± 0.6	7.1 ± 0.8	3.1 ± 0.2	--
3D-LP	87.3 ± 4.7	6.7 ± 1.6	3.0 ± 0.2	2.4 ± 3.8
3D-MP	88.9 ± 2.2	7.0 ± 1.1	3.1 ± 0.2	--
3D-HP	89.0 ± 1.8	7.5 ± 1.4	3.2 ± 0.2	--

Does not include trace elements less than 1%

Table 4

Compressive Modulus (MPa)

Compressive Modulus (Average MPa ± SD)	
3D-LP	3693 ± 27
3D-MP	3522 ± 52 (*)
3D-HP	2579 ± 106 (*^)

Significance $p<0.05$.

* vs. LP,

^ vs. MP